Available online at www.sciencedirect.com
ScienceDirect
Journal of Organometallic Chemistry 692 (2007) 4639–4646
Journal of Organometallic Chemistry
www.elsevier.com/locate/jorganchem

Theoretical investigation on the model active site for isotactic polypropylene in heterogeneous Ziegler–Natta catalyst: A density functional study

Jin Woo Lee, Won Ho Jo *

Hyperstructured Organic Materials Research Center and Department of Materials Science and Engineering, Seoul National University, Seoul 151-742, Republic of Korea

Received 28 March 2007; received in revised form 2 May 2007; accepted 3 May 2007
Available online 18 May 2007

Abstract

The stereoselectivity of the model active site formed by the adsorption of Ti_2Cl_7 on the (1 0 0) surface of $MgCl_2$ was investigated by density functional calculations. The analysis of energetics for successive propylene insertions into the model active site reveals that the insertion of propylene into the model active site is energetically more favorable when a growing chain and one chlorine atom (that makes the active site chiral) are on the opposite side rather than on the same side. From this result, it is realized that the model active site is highly stereoselective. It is also observed that the Cl atoms near the growing chain significantly affect the activation energy barrier through the interaction with the growing chain.

Keywords: Theoretical methods; Density functional theory; Ziegler–Natta catalyst; Isotactic polypropylene; Stereoselectivity

1. Introduction

Since the first synthesis of isotactic polypropylene using Ziegler–Natta (ZN) catalyst in the early 1950s, polymerization with ZN catalyst has been one of the most important industrial methods for the synthesis of polyolefins, especially polypropylene [1,2]. This catalyst has evolved from simple $TiCl_3$ crystals into the current $MgCl_2$-supported catalytic system, which is usually prepared either by comilling $MgCl_2$ and $TiCl_4$ with a Lewis base, or by chemically treating $MgCl_2$ with a Lewis base in the presence of excess $TiCl_4$. Finally, this catalyst is activated by the addition of cocatalyst such as $Al(C_2H_5)_3$.

In preparation of $MgCl_2$-supported ZN catalytic system, the milling process produces different lateral surfaces of $MgCl_2$ on which $TiCl_4$ can coordinate in several ways, resulting in the formation of various active sites which differ in stereoselectivity [3–5]. A number of experimental studies have been performed to investigate the nature of the active sites for improving stereoselectivity of this catalyst [6–32]. As a result, modern ZN catalysts, which have led to the large-scale production of highly isotactic polypropylene, have been developed. Despite these innovations of industrial catalysts achieved predominantly by trial and error, the mechanism of polymerization with ZN catalyst has not yet been fully understood. In particular, due to extremely complex chemical nature of these catalytic systems, the atomic structures of the active sites have been scarcely clarified by experiments, remaining under debate.

As an alternative method, theoretical approach has been used to elucidate the elementary step of olefin insertion in ZN catalyst at a molecular level [33–42]. Although these theoretical studies have provided the basic insight into the ZN-based polymerization process, a realistic description of $MgCl_2$ substrate, which plays a crucial role both in the formation of the active sites and in the polymerization process, has not been modeled in calculation and

* Corresponding author. Tel.: +82 2 880 7192; fax: +82 2 885 1748.
E-mail address: whjpoly@plaza.snu.ac.kr (W.H. Jo).

0022-328X/$ - see front matter © 2007 Elsevier B.V. All rights reserved.
doi:10.1016/j.jorganchem.2007.05.017

therefore the mechanism of stereoselectivity has not been completely elucidated.

Recently, more realistic theoretical studies on the stability of active sites, formed by the adsorption of $TiCl_4$ on both (100) and (110) surfaces of $MgCl_2$, have proposed some plausible active sites [43–48]. In particular, Parrinello and his coworkers [46] have suggested that stable active sites are formed only on the (110) surface. Among various active sites created on the (110) surface, the six-fold site formed by epitactical adsorption of $TiCl_4$ has been proposed as the most stable active site [46,48]. However, according to their report, the five-fold site which is less stable than the six-fold site by about 11 kcal/mol is more reactive than the six-fold site due to lower activation energy when the energy for ethylene and propylene insertion is calculated. Parrinello and his coworkers [49] have also proposed the five-fold site as a highly stereoselective active site, when they investigate the propylene insertion into the five-fold site by using Car-Parrinello molecular dynamics (CPMD). More recently, Flisak and Ziegler [50] have reported that this active site polymerizes propylene monomer with high activity and stereoselectivity, even though one chlorine atom of $TiCl_4$ is replaced by Lewis base.

On the other hand, a systematic density functional theory (DFT) investigation has suggested that $TiCl_3$ molecules can bind together on the (100) surface of $MgCl_2$, resulting in the formation of polynuclear Ti_nCl_{3n} species [44]. Moreover, Corradini and his coworkers [44,51] have suggested that these polynuclear sites would be highly stereoselective, since the polynuclear site has a close analogy with the C_2 symmetric site proposed to be isospecific from the molecular mechanics study on $TiCl_3$-based catalytic system [33–35]. However, this proposal has not been proved experimentally and theoretically yet.

Although these theoretical investigations have provided some significant insight into the nature of the active site, a general agreement on the structure of the stereoselective active site and its stability has not been reached [44,46]. Moreover, theoretical studies have been rarely carried out on the propylene insertion into the active sites formed on the (100) surface of $MgCl_2$. For this reason, we investigate the mechanism of propylene insertion into a model active site formed on the (100) surface of $MgCl_2$ by using DFT calculations, particularly focusing on the stereoselectivity of the model active site. For this purpose, the structures and energetics during successive propylene insertions into the model active site have been systematically analyzed.

2. Computational details

The model active site is generated by the adsorption of Ti_2Cl_7 on the (100) surface of $MgCl_2$, where Ti_2Cl_7 is formed from the reduction of dinuclear Ti_2Cl_8 species (Fig. 1). The (100) surface of $MgCl_2$ was described using a model cluster, Mg_9Cl_{18}. The Mg–Cl distance and the Cl–Mg–Cl angle in the cluster were fixed to 2.49 Å and 90°, respectively, in all calculations. This cluster structure is nearly equal to $MgCl_2$ crystal in the bulk [52].

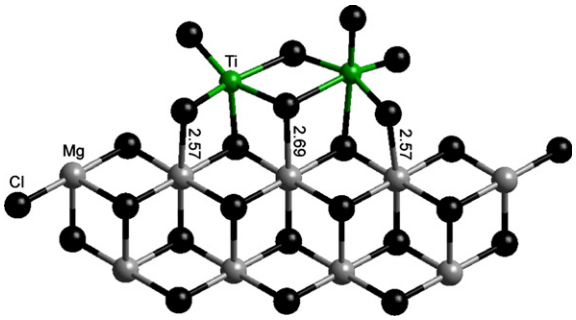

Fig. 1. Geometrically optimized model active site formed by Ti_2Cl_7 adsorption on the (100) surface of $MgCl_2$. The (100) surface of $MgCl_2$ was prepared by using a model cluster, Mg_9Cl_{18}. Only the structure of Ti_2Cl_7 in the model active site has been optimized.

All DFT calculations were carried out using the local potential with the Vosko–Wilk–Nusair (VWN) parameterization [53] corrected in a self-consistent manner by the exchange functional of Becke [54] and the correlation functional of Perdew [55,56] in Amsterdam Density Functional (ADF) package [57–60]. The electronic configurations were described by the triple-ζ Slater type orbital (STO) basis set for Ti and by the double-ζ basis set for Mg, Cl, C and H with a single polarization function for all atoms. The frozen-cores used for DFT calculation are [Ar] for Ti, [Ne] for Mg and Cl, [He] for C. Due to the open-shell character of the model active site, a spin-unrestricted formalism has been used. A geometry optimization was performed using the Broydan–Fletcher–Goldfarb–Shanno (BFGS) energy minimization algorithm [61,62]. The scalar zeroth-order regular approximation (ZORA) method was used for relativistic calculations [63–65].

The propylene insertion follows the Cossee–Arlman mechanism [66–68] revised by Brookhart and Green [69], which is the most accepted reaction mechanism for olefin insertion (Scheme 1). Initially, the active site consists of a Ti atom with an alkyl group and a vacant site for the propylene insertion. Then a propylene monomer occupies the vacancy site, resulting in the formation of π-complex,

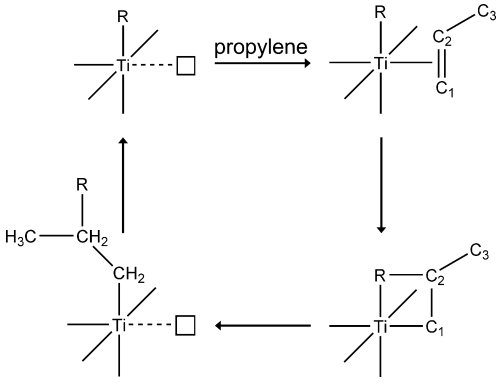

Scheme 1.

which is a local minimum on the energy profile during propylene insertion. From the π-complex, the propylene monomer is inserted by a stepwise decrease of the reaction coordinate, followed by full optimization of geometry with respect to all other degrees of freedom at each step. The reaction coordinate is defined as the distance between the C_α atom (i.e., the carbon which is directly attached to the titanium) and C_2 atom of propylene monomer. The final product is characterized by the minimum energy state with β-agostic interaction.

Upon coordination, prochiral propylene gives rise to non-superposable *re*- and *si*-coordination. According to the definition, isotactic polypropylene is generated by a long series of insertions of propylene with the same enantioface (either *re* or *si*). Therefore, the stereoselectivity of the active site is determined by comparing the energetics during propylene insertion for both enantiofaces. The primary insertion of propylene monomer is only considered because it is experimentally well known that the ZN catalyst is highly regioselective, i.e., the primary insertion is preferred rather than the secondary insertion.

3. Results and discussion

For the insertion of propylene into an active site, a catalytic site has to be activated by a cocatalyst, which results in the formation of Ti-alkyl bond due to the substitution of one dangling Cl coordinated to Ti by an alkyl chain. Fig. 2 shows two possible catalytic species formed from the alkylation of the model active site (in this case, a C_2H_5 group),-which differ in the relative position of the alkyl chain. Catalytic species could be switched between **1** (where the alkyl chain is coordinated away from the $MgCl_2$ surface) and **2** (where the alkyl chain is coordinated close to the $MgCl_2$ surface). DFT calculations show that two catalytic species are isoenergetic and therefore the alkyl chain can occupy two available positions without preference. It is also noteworthy that the two catalytic species exhibit a β-agostic interaction, which is obvious from short Ti–H_β distances (2.07 and 2.08 Å) and an elongated C_β–H_β bond length (1.14 Å) as compared with the normal C–H bond length (1.10 Å).

The two catalytic species have very similar local geometries around the active Ti atom, as shown in Fig. 2. In particular, regardless of the relative position of a growing chain, one chlorine atom (Cl(1) and Cl(5) for the catalytic species **1** and **2**, respectively) makes the active site chiral. This structural similarity leads us to suppose that the energetics and structural features during propylene insertion into one of the two catalytic species are nearly the same with only minor change for the other. For this reason, the insertion of propylene is calculated only for the catalytic species **1** in this study.

3.1. The first insertion of propylene into catalytic species *1*

The first insertion of propylene into the catalytic species **1**, derived from the activation of the model active site, was carried out. The overall behaviors for *re*- and *si*-insertion are similar to each other, as shown in Fig. 3. A propylene monomer is coordinated to the catalytic species **1** without an energy barrier, leading to a π-complex. One interesting feature in the structure of π-complex (for both *re*- and *si*-coordination) is that the C–C bond of a growing chain rotates to the opposite side of the methyl group of the inserting propylene to minimize the repulsive interaction between the growing chain and the inserting propylene monomer, which results in switching from β- to α-agostic interaction, as evidenced by an elongated C_α–H_α distance (1.13 Å). It is also observed that the C=C bond of propylene monomer is almost parallel to the Ti–C_α bond. By decreasing the reaction coordinate, a propylene monomer is inserted into the Ti–C_2H_5 bond via the transition state stabilized by a remarkable α-agostic interaction (the C_α–H_α distance is 1.15 Å). The final product shows a strong β-agostic interaction (the C_β–H_β distance is 1.14 Å).

Despite similar structural features at each stationary point for *re*- and *si*-insertion, the energetics of propylene

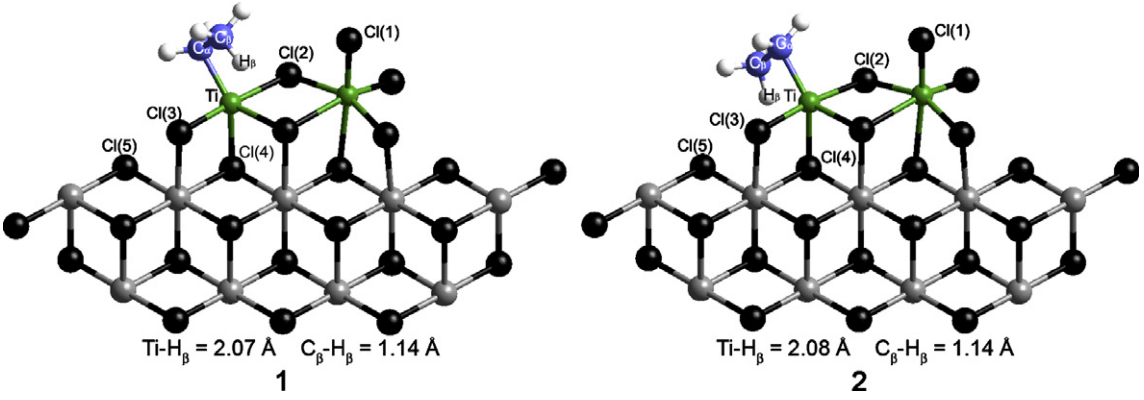

Fig. 2. Optimized structures of the model active site activated by a C_2H_5 molecule. Growing chain is coordinated away from the $MgCl_2$ surface in the catalytic species **1**, whereas the growing chain is coordinated close to the $MgCl_2$ surface in the catalytic species **2**. The energy of **1** is 0.2 kcal/mol higher than **2**.

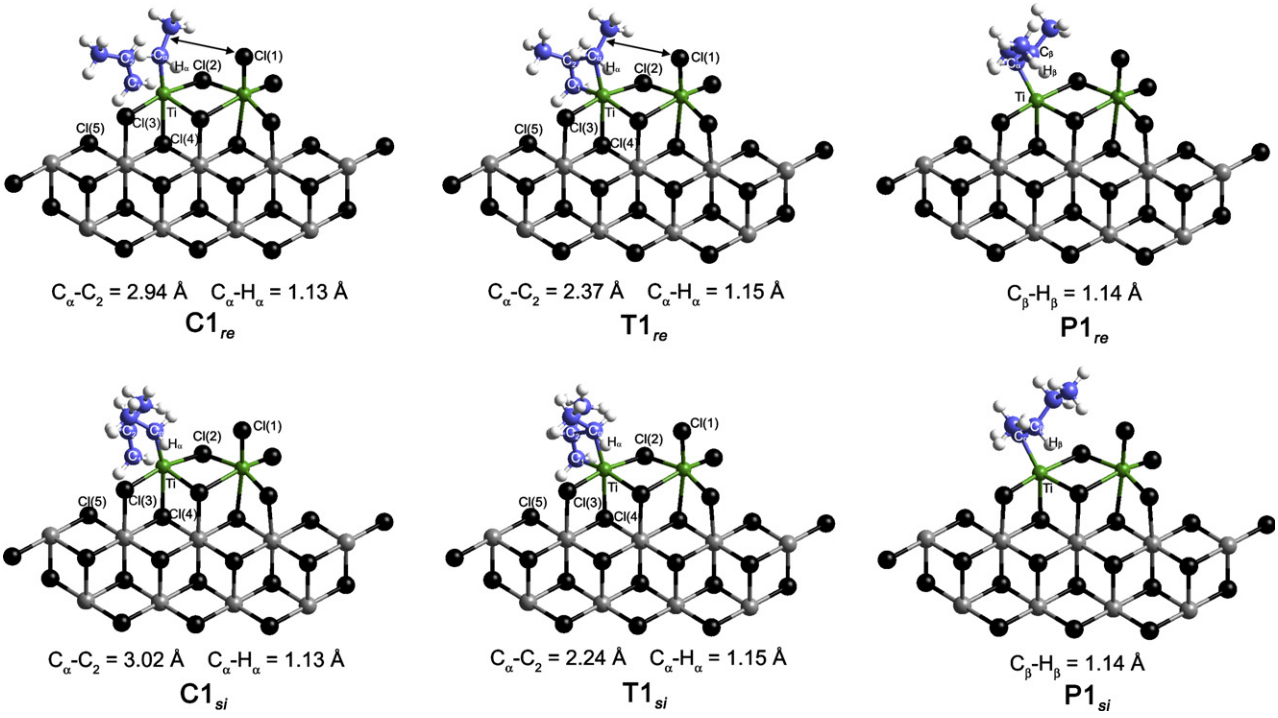

Fig. 3. Structures of the π-complex (**C1**$_{re}$ and **C1**$_{si}$), the transition state (**T1**$_{re}$ and **T1**$_{si}$) and the product (**P1**$_{re}$ and **P1**$_{si}$) during the first insertion of propylene into the catalytic species **1** for *re*- and *si*-insertion, respectively.

insertion is different from each other. The activation energy for *re*-insertion (2.7 kcal/mol) is much lower than that for *si*-insertion (4.8 kcal/mol), although the π-complex for *re*-insertion (**C1**$_{re}$ in Fig. 3) is less stable than that for *si*-insertion (**C1**$_{si}$ in Fig. 3) by 1.1 kcal/mol, as can be seen in Table 1. However, the final product from *re*-insertion is more stable than that from *si*-insertion by 1.0 kcal/mol. This overall energetics indicates that the *re*-insertion is more favorable rather than the *si*-insertion in the first insertion step.

The growing chain for *si*-insertion is located on the opposite side of Cl(1) centering the Ti–C_α–C_2 plane, whereas the growing chain and Cl(1) for *re*-insertion are located on the same side of the Ti–C_α–C_2 plane, as shown in Fig. 3. The orientation of the growing chain observed for *re*-insertion may cause a strong repulsive interaction with Cl(1), and therefore it is expected that the activation energy for *re*-insertion is higher than that for *si*-insertion. In this respect, the lower activation energy calculated for *re*-insertion may not be easily understandable.

To rationalize this unexpected energetics, the interaction energies between the growing chain and Cl atoms (Cl(1) to Cl(3) in Fig. 3) were calculated from the partial atomic charges and the optimized structure of the growing chain and Cl atoms derived from DFT calculation. Fig. 4a–c shows that the growing chain interacts repulsively with each Cl atom, which mainly arises from electrostatic interactions between the negatively charged growing chain and Cl atoms. At the π-complex state, the total repulsive interaction for *re*-insertion is 1.3 kcal/mol higher than that for *si*-insertion (Fig. 4d), which is caused by stronger repulsive interactions between the growing chain and Cl(1), and between the growing chain and Cl(2) in *re*-insertion, as shown in Fig. 4a and b. This stronger repulsive interaction leads to higher energy of **C1**$_{re}$ than **C1**$_{si}$, as listed in Table 1. As a propylene monomer approaches the active site more closely, the repulsive energies decrease slowly until it reaches the transition state, and then the repulsive energies decrease steeply as the transition is passed through. The comparison between the repulsive interaction and the C_α charge reveals that the diminution of repulsive interaction is closely correlated with the decrease of the C_α charge, as shown in Fig. 4d. This reduction in repulsive interaction due to the decrease of the C_α charge may contribute to lower the activation energy. Since the C_α charge decreases steeply at longer reaction coordinate in *re*-insertion (2.37 Å)

Table 1
Energetics for propylene insertion[a]

	Enantioface	π-Complex[b]	Transition state[c]	Product[d]
1st insertion	*re*	−4.7	2.7	−19.9
1st insertion	*si*	−5.8	4.8	−18.9
2nd insertion	*re*	−1.1	–[e]	–[e]
2nd insertion	*si*	−5.7	5.8	−18.6

[a] Energies in kcal/mol.
[b] Relative energy of π-complex with respect to the sum of energies of separated monomer and catalytic species.
[c] Propylene insertion barrier with respect to π-complex.
[d] Relative energy of product with respect to the sum of energies of separated monomer and catalytic species.
[e] Not calculated.

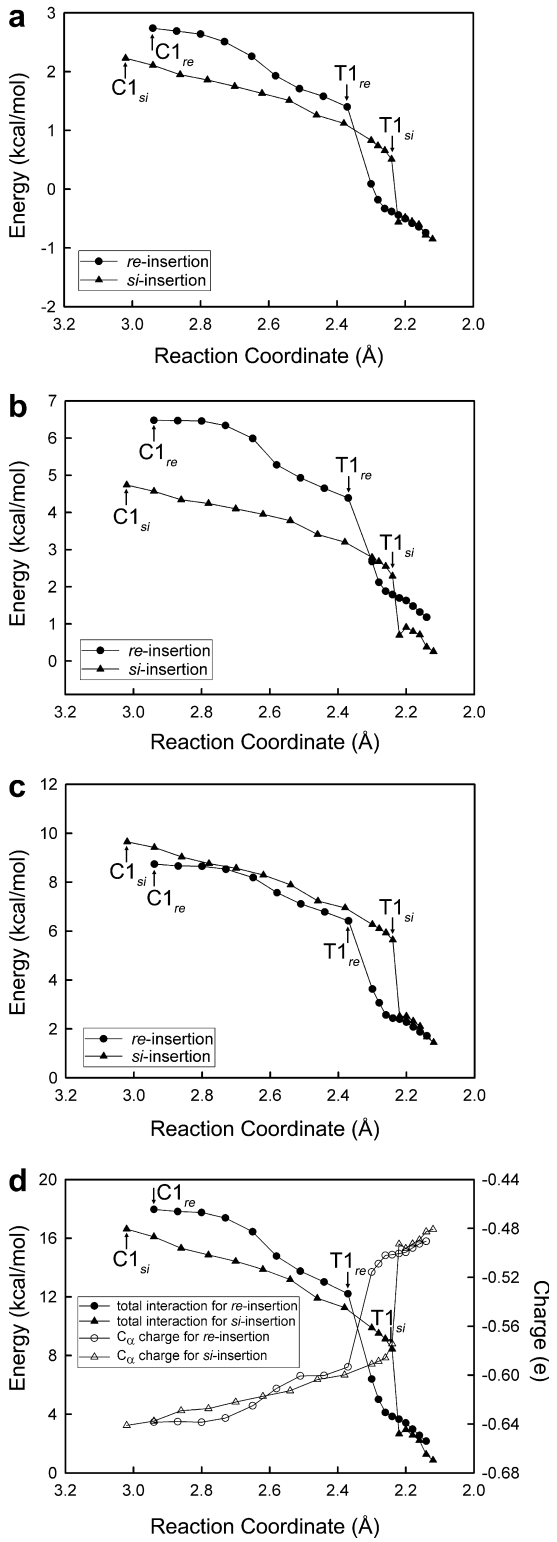

Fig. 4. Interaction energies of a growing chain with each Cl atom (a, b, and c for Cl(1), Cl(2), and Cl(3), respectively) and the total interaction energy between the growing chain and Cl atoms with the partial atomic charge of C_α (d) during the first propylene insertion into the catalytic species **1**.

than in *si*-insertion (2.24 Å), as shown in Fig. 4d, it is conjectured that the lower activation energy for *re*-insertion arises from the larger decrease of the C_α charge.

3.2. The second insertion of propylene into catalytic species *1*

In order to investigate the chain propagation process, the second propylene monomer is inserted into the product ($\mathbf{P1}_{re}$), obtained from the first insertion through energetically more favorable *re*-insertion. The second insertion follows the same reaction pathway as the first insertion, differing slightly only in the orientation of propylene monomer at the π-complex state, as shown in Fig. 5. The larger bulkiness of growing chain, resulted from the first insertion, causes to rotate the inserting propylene monomer to minimize the repulsive interaction between the growing chain and the propylene monomer, which results in orienting the C=C bond of propylene monomer almost perpendicularly to the Ti–C_α bond in *si*-insertion with $\theta = 75.7°$ defined by dihedral angle of C_α–Ti–C_1–C_2 ($\theta = 0°$ when Ti–C_α bond and C_1–C_2 bond are parallel). On the other hand, the rotation of propylene monomer is prohibited in *re*-insertion due to the steric hindrance between the methyl group of propylene monomer and Cl(5) ($\theta = -44.3°$).

In the second insertion, the repulsive interaction between the growing chain and Cl(1) becomes stronger in *re*-insertion due to an increase in bulkiness of the growing chain, which leads to destabilize the active site, as evidenced in an increase in the Ti–Cl(4) distance (3.14 Å) compared with that in *si*-insertion (2.89 Å). As a result, the energy of π-complex for *re*-insertion (−1.1 kcal/mol) is much higher than that for *si*-insertion (−5.7 kcal/mol). This energetics indicates that propylene monomer is not able to form a stable π-complex in *re*-coordination and therefore propylene monomer for the second insertion would be inserted only through *si*-insertion. For this reason, the second insertion of propylene was investigated only for *si*-insertion hereafter.

The structure at each stationary point of the second *si*-insertion of propylene into the $\mathbf{P1}_{re}$ is shown in Fig. 6. During propylene insertion from the π-complex of *si*-coordination ($\mathbf{C2}_{si}$), the inserting propylene monomer rotates to have the C=C bond parallel to the Ti–C_α bond through the rotational transition state $\mathbf{TS\ C2}_{si}$–$\mathbf{C2}^{\#}_{si}$ (3.4 kcal/mol higher than $\mathbf{C2}_{si}$ and $\theta = 56.4°$), which leads to $\mathbf{C2}^{\#}_{si}$ (0.5 kcal/mol lower than $\mathbf{TS\ C2}_{si}$–$\mathbf{C2}^{\#}_{si}$ and $\theta = 29.2°$). By decreasing the reaction coordinate, propylene is inserted through the transition state $\mathbf{T2}_{si}$, which has higher energy than $\mathbf{C2}^{\#}_{si}$ by 2.4 kcal/mol. The overall energy profile in Fig. 7 shows that the activation energy is 5.8 kcal/mol. This activation energy is very close to that of the first insertion (4.8 kcal/mol) and is reasonably in agreement with an experimental result (6.8–9.1 kcal/mol) reported from the propylene insertion into $TiCl_4/MgCl_2$ catalyst [70].

3.3. Stability and stereoselectivity

Recently, the propylene insertion into dinuclear active site formed by Ti_2Cl_6 on the (100) surface of $MgCl_2$ was investigated by using the CPMD [46]. According to the report, Ti_2Cl_6 is adsorbed weakly on the (100) surface of

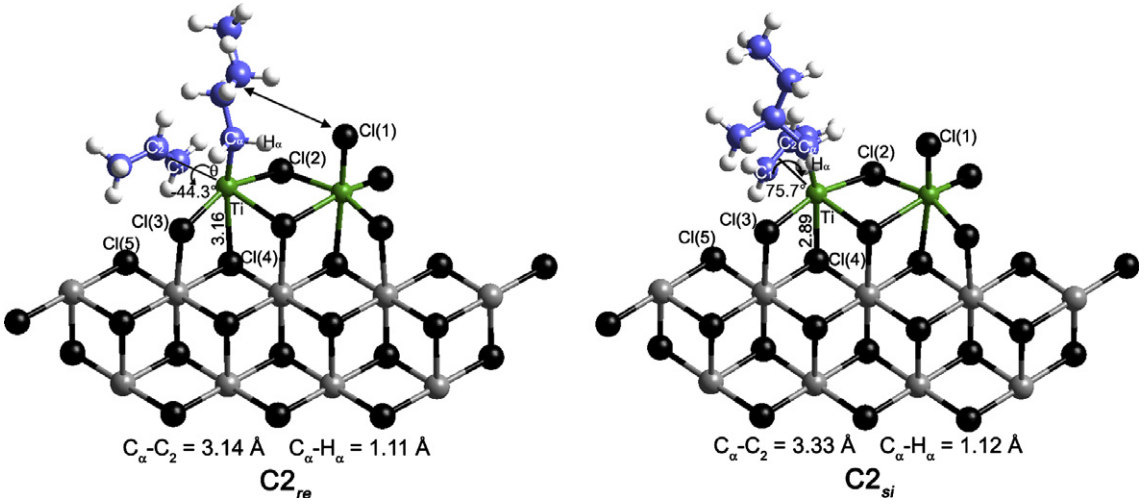

Fig. 5. Structures of the π-complex for the second insertion of propylene into the $\mathbf{P1}_{re}$ for *re*-insertion ($\mathbf{C2}_{re}$) and *si*-insertion ($\mathbf{C2}_{si}$).

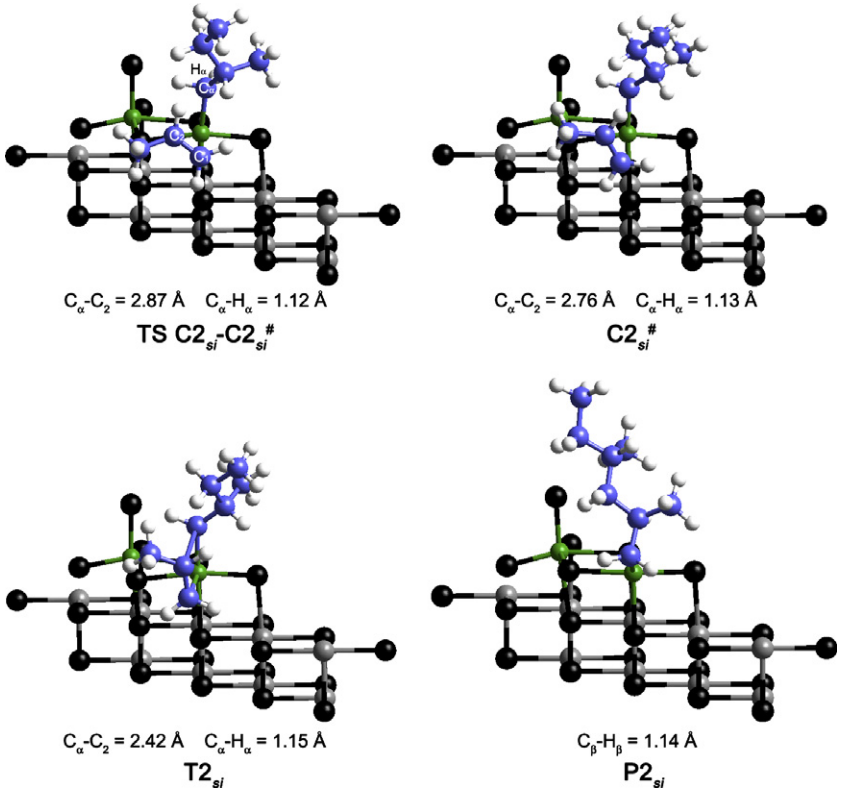

Fig. 6. Structures of rotational intermediates (**TS** $\mathbf{C2}_{si}$–$\mathbf{C2}_{si}^{\#}$ and $\mathbf{C2}_{si}^{\#}$) and the transition state ($\mathbf{T2}_{si}$) during the second insertion of propylene into the $\mathbf{P1}_{re}$ for *si*-insertion.

$MgCl_2$, which is indicated by a long distance between Mg of substrate and Cl of Ti_2Cl_6 (3.07 Å). As a result, the dinuclear active site is disrupted during propylene insertion with one $TiCl_4$ being expelled. In fact, it has been reported that $TiCl_3$ is preferentially adsorbed on the (100) surface of $MgCl_2$ in an isolated form rather than the dinuclear Ti_2Cl_6 form, whereas Ti_2Cl_7 is preferentially adsorbed on the (100) surface of $MgCl_2$ rather than $TiCl_4$ and $TiCl_3$ in an isolated form on the same surface [44]. In our calculation, Ti_2Cl_7 is adsorbed on the (100) surface of $MgCl_2$ with a binding energy of −20.2 kcal/mol and a short Mg–Cl distance (2.57 Å), which agrees well with a previous theoretical result [44].

To investigate the stereoselectivity during propagation of propylene polymerization, the second insertion into the product ($\mathbf{P1}_{si}$), obtained from the first *si*-insertion, was also investigated. As observed in the second insertion into the $\mathbf{P1}_{re}$, when propylene is inserted through

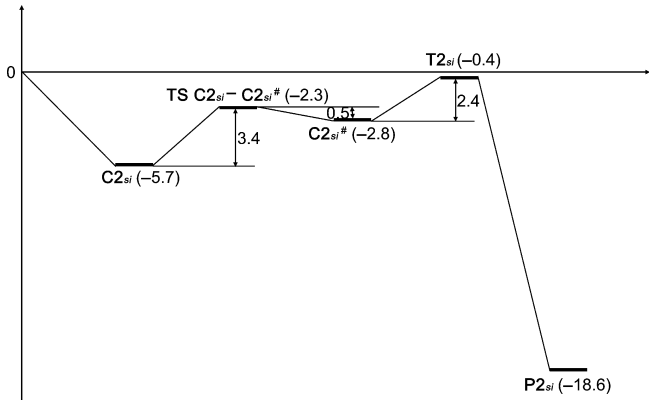

Fig. 7. Energy diagram during the second insertion of propylene into the $\mathbf{P1}_{re}$ for *si*-insertion.

re-coordination, the active site is destabilized due to the strong repulsive interaction between the growing chain and Cl(1), as evidenced in an increase in the Ti–Cl(4) distance (3.13 Å) compared with that in *si*-insertion (2.90 Å) (Fig. 8). As a result, the energy of π-complex for *re*-insertion (−2.2 kcal/mol) is much higher than that for *si*-insertion (−6.4 kcal/mol).

The analysis of energetics for successive propylene insertions into the model active site reveals that regardless of the enantioface for the first insertion, propylene is preferentially inserted when a growing chain is located on the opposite side of one chlorine atom (that makes the active site chiral) in the second insertion, although propylene is preferentially inserted when the growing chain and the chlorine atom are on the same side in the first insertion. This different behavior between the first insertion and the second insertion arises from the bulkiness of growing chain. That is, a propylene monomer in the first insertion is preferentially inserted when the growing chain and the chlorine atom are on the same side, because the repulsive interaction between small growing chain and the chlorine atom is low and the C_α charge decreases steeply earlier. On the other hand, in the second insertion, the repulsive interaction between large growing chain and the Cl atom becomes larger when the growing chain and the chlorine atom are on the same side, which destabilizes the active site and leads to unstable π-complex. Consequently, the growing chain for the second insertion is oriented toward free space region (the opposite side of the chlorine atom) to minimize the repulsive interaction with the Cl atom. This energetics suggests that after the second insertion, propylene monomer is preferentially inserted when the growing chain is located on the opposite side of the chlorine atom, otherwise the repulsive interaction between the growing chain and the Cl atom becomes too large to accommodate the inserting propylene monomer.

4. Conclusions

In this paper, the stereoselectivity of the model active site formed by the adsorption of Ti_2Cl_7 on the (1 0 0) surface of $MgCl_2$ was investigated using DFT calculations. The analysis of energetics for successive propylene insertions into the model active site reveals that a propylene monomer is preferentially inserted when a growing chain is located on the opposite side of one chlorine atom (that makes the active site chiral) during propagation step. The mechanism for stereoselective insertion is that the growing chain is oriented toward free space region to minimize the repulsive interaction between the growing chain and the chlorine atom, which discriminates between two enantiofaces of prochiral propylene. This insertion mechanism is consistent with the growing-chain orientation mechanism proposed by Corradini [33–35,44,51].

To the best of our knowledge, our theoretical study is the first demonstration on the stereoselectivity of the active site formed on the (1 0 0) surface of $MgCl_2$, which may provide a

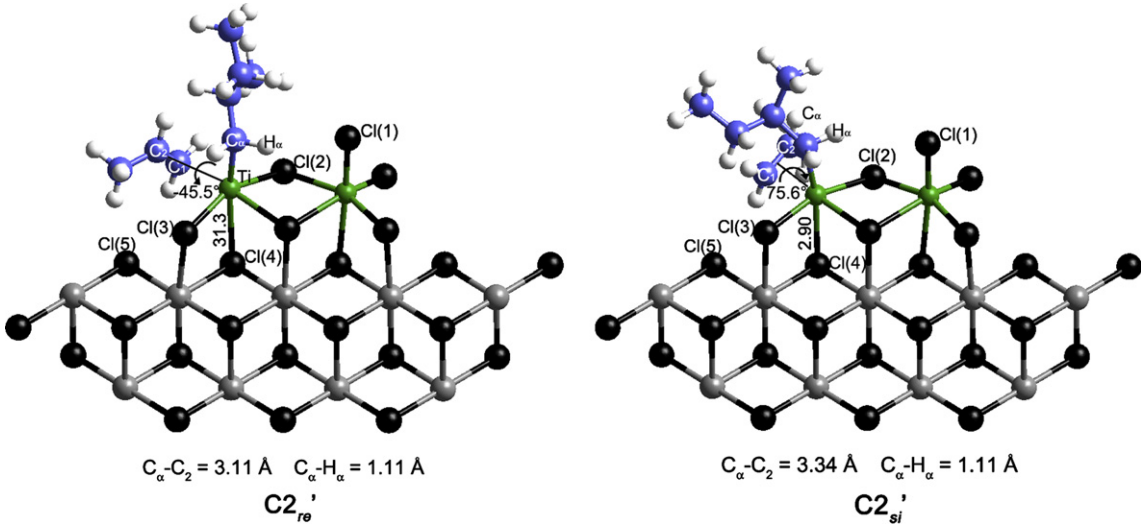

Fig. 8. Structures of the π-complex during the second insertion of propylene into the $\mathbf{P1}_{si}$ for *re*-insertion ($\mathbf{C2'}_{re}$) and *si*-insertion ($\mathbf{C2'}_{si}$).

new insight for the rational molecular design of better ZN catalytic systems.

Acknowledgements

The authors thank the Korea Science and Engineering Foundation (KOSEF) through Hyperstructured Organic Materials Research Center (HOMRC) for their financial support.

References

[1] J. Boor Jr., Ziegler–Natta Catalysts and Polymerizations, Academic Press, New York, 1979.
[2] P.C. Barbé, G. Cecchin, L. Noristi, Adv. Polym. Sci. 81 (1987) 1.
[3] H. Mori, M. Sawada, T. Higuchi, K. Hasebe, N. Otsuka, M. Terano, Macromol. Rapid Commun. 20 (1999) 245.
[4] H. Mori, T. Higuchi, N. Otsuka, M. Terano, Macromol. Chem. Phys. 201 (2000) 2789.
[5] P. Corradini, V. Barone, R. Fusco, G. Guerra, Gazz. Chim. Ital. 113 (1983) 601.
[6] M.C. Sacchi, C. Shan, P. Locatelli, I. Tritto, Macromolecules 23 (1990) 383.
[7] M.C. Sacchi, I. Tritto, C. Shan, R. Mendichi, L. Noristi, Macromolecules 24 (1991) 6823.
[8] M.C. Sacchi, F. Forlini, I. Tritto, P. Locatelli, G. Morini, L. Noristi, E. Albizzati, Macromolecules 29 (1996) 3341.
[9] G. Morini, E. Albizzati, G. Balbontin, I. Mingozzi, M.C. Sacchi, F. Forlini, I. Tritto, Macromolecules 29 (1996) 5770.
[10] H. Mori, K. Hasebe, M. Terano, J. Mol. Catal. A 140 (1999) 165.
[11] H. Mori, M. Endo, M. Terano, J. Mol. Catal. A 145 (1999) 211.
[12] H. Matsuoka, B. Liu, H. Nakatani, M. Terano, Macromol. Rapid Commun. 22 (2001) 326.
[13] B. Liu, T. Nitta, H. Nakatani, M. Terano, Macromol. Symp. 213 (2004) 7.
[14] Q. Wang, N. Murayama, B. Liu, M. Terano, Macromol. Chem. Phys. 206 (2005) 961.
[15] J.C. Chadwick, G. Morini, G. Balbontin, I. Camurati, J.J.R. Heere, I. Mingozzi, F. Testoni, Macromol. Chem. Phys. 202 (2001) 1995.
[16] J.C. Chadwick, Macromol. Symp. 173 (2001) 21.
[17] A.K. Yaluma, P.J.T. Tait, J.C. Chadwick, J. Polym. Sci. Part A: Polym. Chem. 44 (2006) 1635.
[18] J. Xu, L. Feng, S. Yang, Macromolecules 30 (1997) 2539.
[19] J. Xu, L. Feng, S. Yang, Y. Yang, X. Kong, Macromolecules 30 (1997) 7655.
[20] E. Albizzati, U. Giannini, G. Balbontin, I. Camurati, J.C. Chadwick, T. Dall'occo, Y. Dubitsky, M. Galimberti, G. Morini, A. Maldotti, J. Polym. Sci. Part A: Polym. Chem. 35 (1997) 2645.
[21] J.C. Chadwick, G. Morini, G. Balbontin, I. Mingoui, E. Albizzati, O. Sudmeijer, Macromol. Chem. Phys. 198 (1997) 1181.
[22] V. Busico, R. Cipullo, G. Talarico, A.L. Segre, J.C. Chadwick, Macromolecules 30 (1997) 4786.
[23] V. Busico, R. Cipullo, G. Monaco, G. Talarico, M. Vacatello, J.C. Chadwick, A.L. Segre, O. Sudmeijer, Macromolecules 32 (1999) 4173.
[24] V. Busico, R. Cipullo, C. Polzone, G. Talarico, J.C. Chadwick, Macromolecules 36 (2003) 2616.
[25] V. Busico, J.C. Chadwick, R. Cipullo, S. Ronca, G. Talarico, Macromolecules 37 (2004) 7437.
[26] J.C. Chadwick, F.P.T.J. van der Burgt, S. Rastogi, V. Busico, R. Cipullo, G. Talarico, J.J.R. Heere, Macromolecules 37 (2004) 9722.
[27] Y.V. Kissin, F.M. Mirabella, C.C. Meverden, J. Polym. Sci. Part A: Polym. Chem. 43 (2005) 4351.
[28] E. Magni, G.A. Somorjai, J. Phys. Chem. B 102 (1998) 8788.
[29] S.H. Kim, G.A. Somorjai, J. Phys. Chem. B 104 (2000) 5519.
[30] S.H. Kim, G.A. Somorjai, J. Phys. Chem. B 105 (2001) 3922.
[31] S.H. Kim, G.A. Somorjai, J. Phys. Chem. B 106 (2002) 1386.
[32] J.C. Randall, Macromolecules 30 (1997) 803.
[33] P. Corradini, V. Barone, R. Fusco, G. Guerra, Eur. Polym. J. 15 (1979) 1133.
[34] P. Corradini, G. Guerra, R. Fusco, V. Barone, Eur. Polym. J. 16 (1980) 835.
[35] P. Corradini, V. Barone, G. Guerra, Macromolecules 15 (1982) 1242.
[36] H. Fujimoto, T. Yamasaki, H. Mizutani, N. Koga, J. Am. Chem. Soc. 107 (1985) 6157.
[37] F.U. Axe, J.M. Coffin, J. Phys. Chem. 98 (1994) 2567.
[38] S. Sakai, J. Phys. Chem. 98 (1994) 12053.
[39] P. Margl, L. Deng, T. Ziegler, Organometallics 17 (1998) 933.
[40] L. Cavallo, G. Guerra, P. Corradini, J. Am. Chem. Soc. 120 (1998) 2428.
[41] P. Margl, L. Deng, T. Ziegler, J. Am. Chem. Soc. 120 (1998) 5517.
[42] V. Virkkunen, L. Pietila, F. Sundholm, Polymer 44 (2003) 3133.
[43] J.D. Gale, C.R.A. Catlow, M.J. Gillan, Top. Catal. 9 (1999) 235.
[44] G. Monaco, M. Toto, G. Guerra, P. Corradini, L. Cavallo, Macromolecules 33 (2000) 8953.
[45] C. Martinsky, C. Minot, J.M. Ricart, Surf. Sci. 490 (2001) 237.
[46] M. Boero, M. Parrinello, H. Weiss, S. Hüffer, J. Phys. Chem. A 105 (2001) 5096.
[47] M. Seth, P.M. Margl, T. Ziegler, Macromolecules 35 (2002) 7815.
[48] M. Boero, M. Parrinello, K. Terakura, J. Am. Chem. Soc. 120 (1998) 2746.
[49] M. Boero, M. Parrinello, S. Hüffer, H. Weiss, J. Am. Chem. Soc. 122 (2000) 501.
[50] Z. Flisak, T. Ziegler, Macromolecules 38 (2005) 9865.
[51] P. Corradini, G. Guerra, L. Cavallo, Acc. Chem. Res. 37 (2004) 231.
[52] D.E. Partin, M. O'Keeffe, J. Solid State Chem. 95 (1991) 176.
[53] S.H. Vosko, L. Wilk, M. Nusair, Can. J. Phys. 58 (1980) 1200.
[54] A. Becke, Phys. Rev. A 38 (1988) 3098.
[55] J.P. Perdew, Phys. Rev. B 33 (1986) 8822.
[56] J.P. Perdew, Phys. Rev. B 34 (1986) 7406.
[57] E.J. Baerends, D.E. Ellis, P. Ros, Chem. Phys. 2 (1973) 41.
[58] C.F. Guerra, J.G. Snijders, G. te Velde, E.J. Baerends, Theor. Chem. Acc. 99 (1998) 391.
[59] G. te Velde, E.J. Baerends, Comput. Phys. 99 (1992) 84.
[60] L. Versluis, T. Ziegler, J. Chem. Phys. 88 (1988) 322.
[61] P. Pulay, J. Comput. Chem. 3 (1982) 556.
[62] P. Csaszar, P. Pulay, J. Mol. Struct. 114 (1984) 31.
[63] E. van Lenthe, E.J. Baerends, J.G. Snijders, J. Chem. Phys. 99 (1993) 4597.
[64] E. van Lenthe, E.J. Baerends, J.G. Snijders, J. Chem. Phys. 101 (1994) 9783.
[65] E. van Lenthe, A. Ehlers, E.J. Baerends, J. Chem. Phys. 110 (1999) 8943.
[66] P. Cossee, J. Catal. 3 (1964) 80.
[67] E. Arlman, J. Catal. 3 (1964) 89.
[68] E. Arlman, P. Cossee, J. Catal. 3 (1964) 99.
[69] M. Brookhart, M.L.H. Green, J. Organomet. Chem. 250 (1983) 395.
[70] J.C. Chien, P. Bres, J. Polym. Sci., Polym. Chem. Ed. 24 (1986) 1967.